applied sciences

MDPI

Article

Investigation on the Differential Quadrature Fabry–Pérot Interferometer with Variable Measurement Mirrors

Yi-Chieh Shih [1,*], Pi-Cheng Tung [1], Wen-Yuh Jywe [2], Chung-Ping Chang [3], Lih-Horng Shyu [4] and Tung-Hsien Hsieh [2]

1 Department of Mechanical Engineering, National Central University, Taoyuan 320, Taiwan; t331166@ncu.edu.tw
2 Smart Machinery and Intelligent Manufacturing Research Center, National Formosa University, Yunlin 632, Taiwan; jywe@nfu.edu.tw (W.-Y.J.); p98951078@nfu.edu.tw (T.-H.H.)
3 Department of Mechanical and Energy Engineering, National Chiayi University, Chiayi 600, Taiwan; cpchang@mail.ncyu.edu.tw
4 Department of Electro-Optical Engineering, National Formosa University, Yunlin 632, Taiwan; lhshyu@nfu.edu.tw
* Correspondence: 105383003@cc.ncu.edu.tw

Received: 7 July 2020; Accepted: 4 September 2020; Published: 6 September 2020



Abstract: Due to the common path structure being insensitive to the environmental disturbances, relevant Fabry–Pérot interferometers have been presented for displacement measurement. However, the discontinuous signal distribution exists in the conventional Fabry–Pérot interferometer. Although a polarized Fabry–Pérot interferometer with low finesse was subsequently proposed, the signal processing is complicated, and the nonlinearity error of sub-micrometer order occurs in this signal. Therefore, a differential quadrature Fabry–Pérot interferometer has been proposed for the first time. In this measurement system, the nonlinearity error can be improved effectively, and the DC offset during the measurement procedure can be eliminated. Furthermore, the proposed system also features rapid and convenient replacing the measurement mirrors to meet the inspection requirement in various measuring ranges. In the comparison result between the commercial and self-developed Fabry–Pérot interferometer, it reveals that the maximum standard deviation is less than 0.120 μm in the whole measuring range of 600 mm. According to these results, the developed differential Fabry–Pérot interferometer is feasible for precise displacement measurement.

Keywords: differential Fabry–Pérot interferometer; homodyne interferometer; nonlinearity error; linear displacement

1. Introduction

From the comparison between the resolution and measuring range of different measurement devices, high resolution and contactless measurement can be realized by the laser interferometer in various measuring ranges. Hence, the industrial application, including the calibration of the linear axis for the machine tool, the positioning of the microelectromechanical equipment, and the wafer dicing, must rely on it to ensure the quality of production and the high-precision inspection requirement [1–4].

Currently, the Michelson interferometer is the primary tool for displacement measurement in a large dynamic range. In the optical structure, the laser beam is divided into a reference beam and a measurement beam by a non-polarizing beam splitter (BS), and corresponding mirrors reflect each beam and then form the interferometric signal. The phase of this signal depends on the optical path difference between the reference beam and the measurement beam. Because the reference path is separate from

the measurement path, this kind of interferometer is susceptible to relative environmental changes. In contrast, the Fabry–Pérot interferometer is based on the common path structure. For this reason, laser beams propagate in the same optical path, and this interferometer possesses high resistance of environmental disturbances that contain thermal expansion, micro-flow gradient, and the tiny vibration [5–7].

The optical arrangement of the conventional Fabry–Pérot interferometer, which contains a laser light source, a detector, and an optical cavity composed of two plane mirrors (PMs) had been proposed by Charles Fabry and Alfred Pérot in 1897 (illustrated in Figure 1a) [8]. The laser light source is incident into the optical cavity in a nearly vertical direction, and the laser beam is divided into numerous transmitted beams from the cavity reciprocally. Then the interferometric signal can be acquired by the detector. Because the optical cavity of the conventional Fabry–Pérot interferometer is composed of two PMs with a high reflectance, which results in the discontinuous signal distribution with high finesse. Furthermore, displacement or vibration can only be realized by the fringe counting method, and it is rarely utilized in large-scale dynamic displacement measurements.

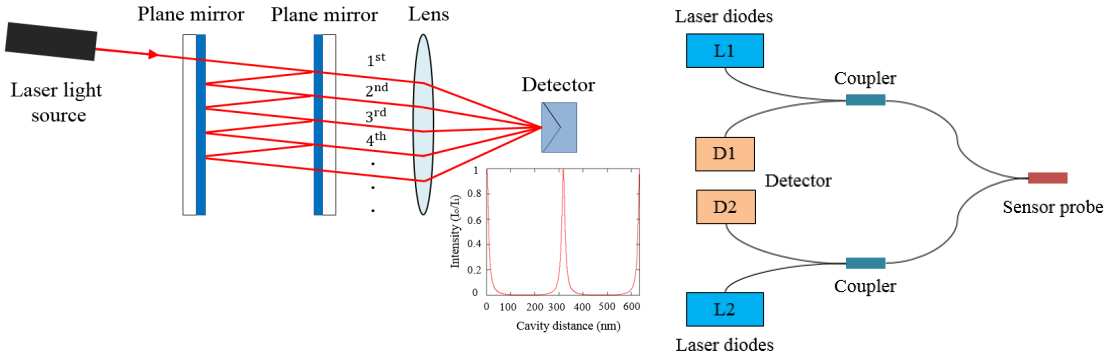


Figure 1. Optical arrangement of Fabry–Pérot interferometer: (**a**) Conventional structure, and (**b**) quadrature phase-shifted fiber-optic structure.

According to the development of the optical encoder and the interferometer system, to improve the measurement accuracy, correlated technologies, including orthogonal signal processing and signal subdivision, have been proposed. Therefore, the quadrature phase-shifted fiber-optic Fabry–Pérot interferometer demonstrated in Figure 1b had been presented by Kent A. Murphy et al. in 1999 [9]. This structure is based on the spatial phase-shifted method to form the orthogonal signal, which will be obtained by two detectors (D_1, D_2). The phase shift is mainly decided by the position and angle of the probe and the measured surface. For this reason, the measuring range is limited by the performance of the optical-mechanical alignment.

In the recent study, polarized Fabry–Pérot interferometer with low finesse, shown in Figure 2, had been proposed by Chang et al. in 2013 [10,11]. The octadic-wave plate is placed in the optical cavity, and its polarization axis must be the same as that of the polarizing beam splitter (PBS) to introduce the orthogonal phase shift between two interferometric signals. By reducing the reflectance of the plane mirror, continuous signal distribution can be acquired, and the interferometric signals (I_s, I_p) can be detected by the photodiodes (PD_1, PD_2). The orthogonal interferometric signal, shown in Figure 3a, can be expressed by Equations (1) and (2) [12], where A_0 is the amplitude of the incident beam, R and T are the reflectance and transmittance of the coated plane mirror, T′ is the transmittance of the optical cavity, and δ is the phase difference. In the simulation, optical parameters of R, T, and T′ are 0.25, 0.75, and 0.86, respectively. The analysis method of the mean normalization is adopted to evaluate the amplitude and DC offset of the orthogonal signal in this study. Theoretically, if the signal amplitude is uniform change and there is no DC offset existing, the center (offset) of the orthogonal signal will

be at the zero points, and it will become a circle shape after the mean normalization processing. Interferometric signals (I_s, I_p) can be processed by the mean normalization ($I_{s\text{-}nom}$, $I_{p\text{-}nom}$) individually represented in Equations (3) and (4). Then, the normalized orthogonal signal illustrated in Figure 3b can be obtained, where I_max, I_min, and μ are the maximum, minimum, and average intensity.

$$I_s = \frac{\frac{1}{2}A_0{}^2 \times T^2 \times T'}{1 + R^2 \times T'^2 - 2 \times T' \times R \times \cos\left(\delta - \frac{\pi}{4}\right)} \quad (1)$$

$$I_p = \frac{\frac{1}{2}A_0{}^2 \times T^2 \times T'}{1 + R^2 \times T'^2 - 2 \times T' \times R \times \cos\left(\delta + \frac{\pi}{4}\right)} \quad (2)$$

$$I_{s-nom} = \frac{I_s - \mu}{I_{s_max} - I_{s_min}} \quad (3)$$

$$I_{p-nom} = \frac{I_p - \mu}{I_{p_max} - I_{p_min}} \quad (4)$$

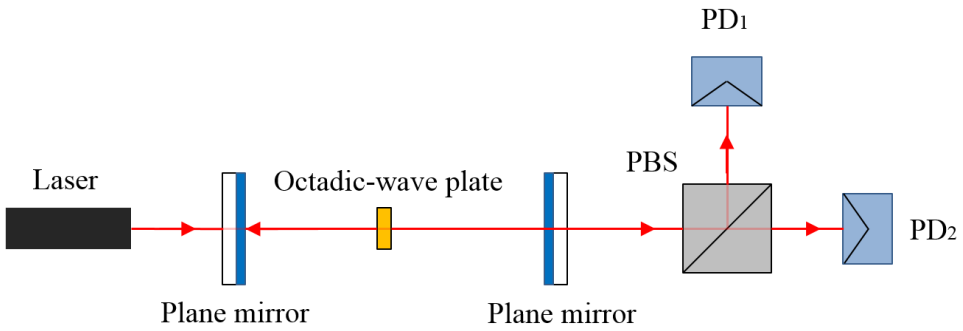
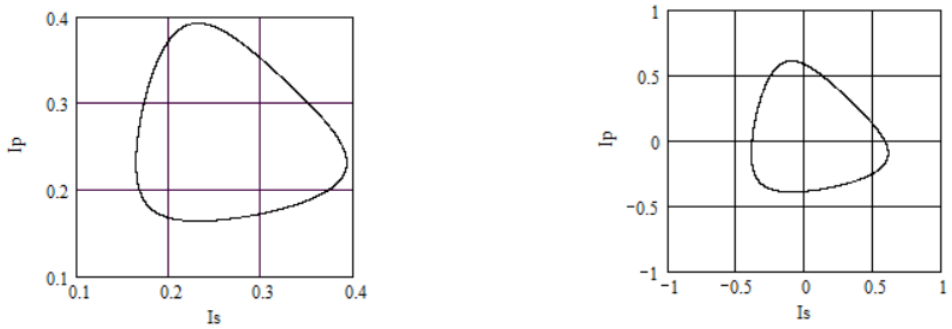


Figure 2. The optical arrangement of polarized Fabry–Pérot interferometer. PBS, polarizing beam splitter; PD, photodiode.



(**a**) (**b**)

Figure 3. Orthogonal signal of polarized Fabry–Pérot interferometer. (**a**) Original signal; (**b**) signal with mean normalization processing.

In this structure, there are two critical issues, including the existing large nonlinearity error in the signal and involving the complex signal processing for the elimination of the direct current (DC) offset. The nonlinearity error is caused by the DC offset, unequal alternating current (AC) amplitudes, and quadrature phase errors that occur in the orthogonal signal. In the simulation results in Figure 3, the orthogonal signal after the mean normalization processing reveals that the signal possesses the DC offset and unequal AC amplitudes, which will lead to the nonlinearity error. Therefore, the measurement accuracy of this measurement structure will be affected by the nonlinearity

error during the measurement. The formula for the analysis of the nonlinearity error is revealed in Equation (5), where I_x and I_y are the interferometric signals, ψ represents the ideal phase, and m is a constant [13–15].

$$\text{Nonlinearity error} = \arctan\left(I_y/I_x\right) - \psi + m\pi \quad (5)$$

In accordance with the measurement structure of the polarized Fabry–Pérot interferometer, the analysis of the nonlinearity error is based on the simulated orthogonal signal, shown in Figure 3. The simulation result (Figure 4) reveals that the nonlinearity error is ranging from −48 to 131 nm in the polarized Fabry–Pérot interferometer.

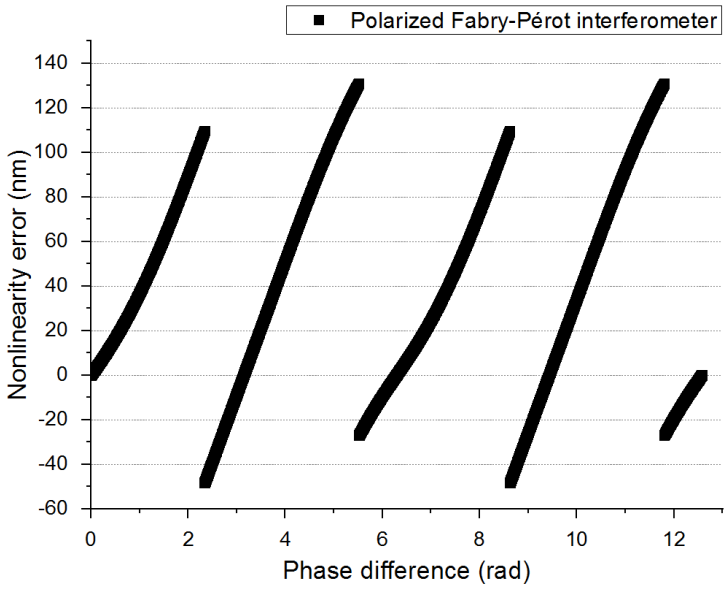


Figure 4. Nonlinearity error of polarized Fabry–Pérot interferometer.

For subsequent signal subdivision, significant interpolation error will occur. Furthermore, the conventional correction method of nonlinearity error is also difficult to implement in this signal [16,17]. Subsequently, a look-up table method was provided to carry out the signal subdivision with the resolution of 0.1 nm in the polarized Fabry–Pérot interferometer [18]. Still, this method can only be processed for a single Lissajous signal under specific measurement conditions, e.g., measuring speed and range, etc. If the measurement signal changes, this method will not be able to carry out. In the correlated study, the Lissajous signal of the start-point and the endpoint in the whole measuring range of 500 mm is different, which means that the signal phase and amplitude are changing [11]. If this signal processing method is utilized in this situation, the inherent measurement performance with the resolution of 0.1 nm will not be achieved in the actual experiment. Furthermore, to avoid the signal drift during the measurement procedure, the DC offset compensation module is also introduced in the polarized Fabry–Pérot interferometer. The conversion of analog to digital and digital to analog is performed in real-time to acquire the signal center and then is to eliminate the DC offset. Since signal processing involves more complex feedback control, if the noise occurs during the measurement, the measurement accuracy will be affected severely. Therefore, this kind of interferometer cannot be performed in high precision and high-speed industrial applications.

By reviewing the development of the Fabry–Pérot interferometer employed for the displacement measurement, the major problems in critical structures are summarized in Table 1. Therefore, how to provide a measurement system based on the Fabry–Pérot interferometer with high measurement performance for employing in the large range is an essential issue. From the above-mentioned description, a differential quadrature Fabry–Pérot interferometer with variable measurement mirrors employing in different measuring ranges is proposed in this study. By the integration of the differential

optical structure and the Fabry–Pérot interferometric technique, the nonlinearity error can be improved effectively, and the DC offset can also be eliminated during the measurement process to realize high precision measurement performance conveniently and flexibly.

Table 1. Comparison between the previous Fabry–Pérot interferometers.

Fabry–Pérot Interferometer / Item	Signal Distribution	Signal Processing Method	Problems
Conventional structure — Reference 8	Discontinuous (high finesse)	Fringe counting	Not suitable for dynamic measurement in large range
Polarized structure — Reference 11	Continuous (low finesse)	Quadrature-based sensing with 2 photodiodes	1. With large nonlinearity error 2. Involved with the complex signal processing

2. Proposed Differential Quadrature Fabry–Pérot Interferometer

Based on the pending patent (application number: 108142443), the optical structure of the proposed differential quadrature Fabry–Pérot interferometer is extended and realized experimentally. It enables the arrangement with two measurement types simultaneously for determining the linear displacement. This structure contains a laser source, an optical cavity, and an optical element and signal sensing module (Figure 5a). The laser beam is incident to the optical cavity module from the laser source module and the optical element and signal sensing module. Then the laser beam is divided into multiple beams and output from the cavity, and PDs placed in the optical element and signal sensing module will inspect the interferometric signals. The laser source module is composed of the high stabilized He-Ne laser and the optical isolator. The purpose of placing the optical isolator is to avoid the laser beam to reflect back from other optical components. The optical cavity module contains two measurement types depending on the selection of different measurement mirrors (Figure 5b). One is the PM type whose optical cavity is composed of two PMs, and the other is the corner cube retro-reflector (CCR) type whose optical cavity consists of a PM and a CCR. In the CCR type, due to its folded measurement structure, the optical resolution can be improved by a factor of two compared to the type of the PM [19]. In addition, owing to CCR bearing large tilt angles of the measurement mirror, this type is more suitable for the displacement measurement within the large range. Due to the multi-beam interferometric measurement structure, the incident beam travels forward and backward in the cavity and is divided into numerous reflected beams (order number of beam: 1st, 2nd, 3rd ... Nth). The Nth beam will pass through the quarter-wave plate twice more than the N-1th beam, so the polarization direction of each laser beam will be orthogonally converted. Then they will be transmitted back to the optical element and signal sensing module. In the optical element and signal sensing module, it contains a quarter-wave plate, two BS, two PBS, and four PDs. According to the proposed optical structure, the interferometric signal can be acquired by PDs for further displacement measurement.

The linearly polarized laser beam with a polarization direction angle of $-\pi/4$ with respect to the y-axis will be acquired after passing through the optical isolator, and it is converted to the right-handed circularly polarized beam by the first quarter-wave plate, whose fast axis is along the y-axis. Then the laser beam will be incident to the BS_1 and the optical cavity. In this cavity, the beam is transmitted to the second quarter-wave plate whose fast axis is at a zero angle with respect to the y-axis multiple times. Numerous reflected laser beams output by the optical cavity are sequentially converted into the orthogonally polarized beams (Figure 5c). The backward laser beam is split into two beams by BS_2, and then each beam is transmitted to the PBS_1 and the PBS_2, respectively. The optical axis of the PBS_2 is rotated around the incident beam by $\pi/4$ relative to that of PBS_1. In the optical arrangement, two pairs of the interferometric signal with a phase difference of π can be obtained. And by subtracting each pair signal, the orthogonal signal for displacement measurement will be determined.

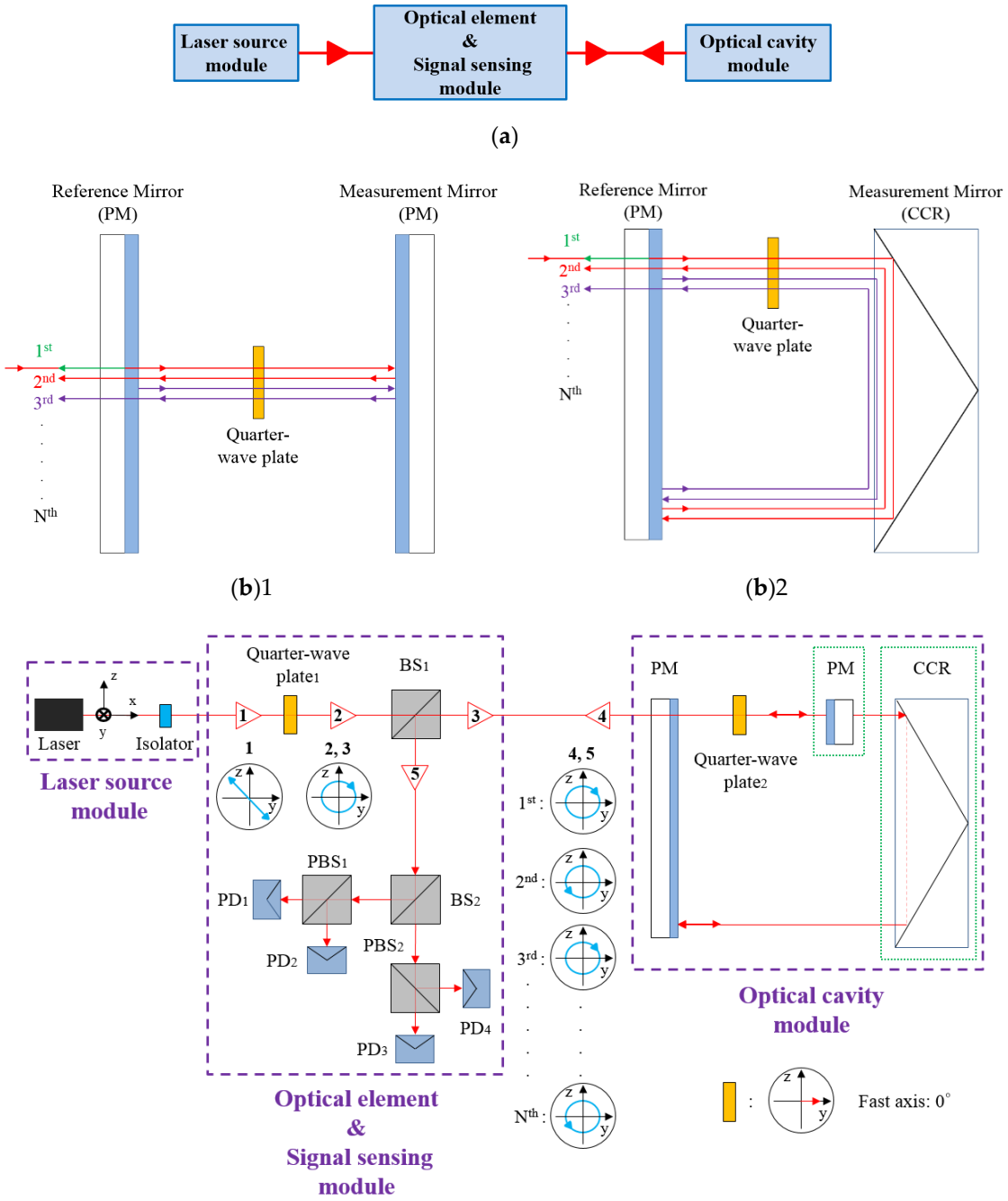


Figure 5. Proposed differential quadrature Fabry–Pérot interferometer: (**a**) Structure composition; (**b**) transmission of laser beams in two measurement types (**b**)1 plane mirrors (PM) type, (**b**)2 cube retro-reflector (CCR) type, (**c**) optical arrangement and the polarization direction of laser beams. PD, photodiode, PBS, polarizing beam splitter; BS, non-polarizing beam splitter.

The Jones matrix of the incident beam and the relevant optical elements in this structure is as Equation (6) to Equation (11).

$$E_{(\Phi)} = \begin{pmatrix} \cos\Phi \\ \sin\Phi \end{pmatrix} \tag{6}$$

$$PF = e^{i\cdot\delta} = e^{i\cdot\frac{4\pi nd}{\lambda}} \tag{7}$$

$$\mathrm{BS} = \frac{1}{\sqrt{2}} \cdot \begin{pmatrix} 1 & 0 \\ 0 & 1 \end{pmatrix} \tag{8}$$

$$\mathrm{QWP}(\theta) = \begin{pmatrix} \cos(\theta) & -\sin(\theta) \\ \sin(\theta) & \cos(\theta) \end{pmatrix} \cdot \begin{bmatrix} e^{-i\cdot\left(\frac{\pi}{4}\right)} & 0 \\ 0 & e^{i\cdot\left(\frac{\pi}{4}\right)} \end{bmatrix} \cdot \begin{pmatrix} \cos(\theta) & \sin(\theta) \\ -\sin(\theta) & \cos(\theta) \end{pmatrix} \tag{9}$$

$$\mathrm{PBS_o}(\alpha) = \begin{pmatrix} \sin(\alpha)^2 & -\sin(\alpha)\cdot\cos(\alpha) \\ -\sin(\alpha)\cdot\cos(\alpha) & \cos(\alpha)^2 \end{pmatrix} \tag{10}$$

$$\mathrm{PBS_e}(\alpha) = \begin{pmatrix} \cos(\alpha)^2 & \sin(\alpha)\cdot\cos(\alpha) \\ \sin(\alpha)\cdot\cos(\alpha) & \sin(\alpha)^2 \end{pmatrix} \tag{11}$$

Where E (Φ) is the electric field of the linearly polarized laser beam after traveling the optical isolator, the angle of the polarization direction with respect to the *y*-axis is Φ. PF is defined as the phase factor ($e^{i\cdot\delta}$) accounts for the optical phase difference (δ) caused by the changing of the cavity distance (d). δ equals 4πnd/λ, where λ is the laser wavelength, and n is the refractive index. For the type of the plane mirror and the corner cube retro-reflector, the optical phase difference equals to 4πnd/λ (δ) and 8πnd/λ (2δ), respectively. BS is the matrix of the non-polarizing beam splitter, and QWP (θ) represents a matrix that corresponds to a quarter-wave plate whose fast axis is at an angle θ with respect to the *y*-axis. $\mathrm{PBS_o}$ (α) and $\mathrm{PBS_e}$ (α) represent two separated beams rotated by an angle α relative to the *x*-axis.

The sum of the electric field can be express as Equation (12), where R and T are the reflectance and transmittance of the coated plane mirror, respectively, Q is the transmittance of the optical cavity, and N is the order number of the backward reflected beam.

$$\mathrm{E_{sum}} = \left[\mathrm{BS}^3\cdot\sqrt{\mathrm{R}} + \mathrm{BS}^3\cdot\left(\sqrt{\mathrm{T}}\right)^2\cdot\sum_{\mathrm{N}=2}^{\infty}\left(\sqrt{\mathrm{R}}\right)^{2\mathrm{N}-3}\cdot\mathrm{Q}^{\mathrm{N}-1}\cdot\mathrm{PF}^{\mathrm{N}-1}\cdot\mathrm{QWP}(\theta_2)^{2\cdot\mathrm{N}-2}\right]\cdot\mathrm{QWP}(\theta_1)\cdot\mathrm{E}(\Phi) \tag{12}$$

For $\mathrm{PD_1}$ to $\mathrm{PD_4}$, the corresponding electric fields of each incident beam are shown from Equation (13) to Equation (16).

$$\mathrm{E_1} = \mathrm{PBS_o}(\alpha_1)\cdot\mathrm{E_{sum}} \tag{13}$$

$$\mathrm{E_2} = \mathrm{PBS_e}(\alpha_1)\cdot\mathrm{E_{sum}} \tag{14}$$

$$\mathrm{E_3} = \mathrm{PBS_o}(\alpha_2)\cdot\mathrm{E_{sum}} \tag{15}$$

$$\mathrm{E_4} = \mathrm{PBS_e}(\alpha_2)\cdot\mathrm{E_{sum}} \tag{16}$$

The light intensity can be expressed as Equation. (17) and two orthogonal signals can be determined by Equation (18) and Equation (19).

$$\mathrm{I} = \mathrm{E}\cdot\mathrm{E}^* \tag{17}$$

$$\mathrm{I_x} = \mathrm{I_1} - \mathrm{I_2} \tag{18}$$

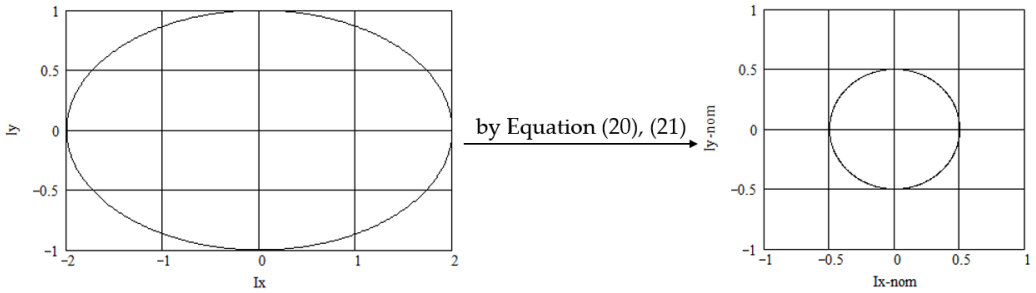
$$\mathrm{I_y} = \mathrm{I_3} - \mathrm{I_4} \tag{19}$$

For the proposed differential measurement structure, the mean normalization processing is similar to the analysis method in the polarized Fabry–Pérot interferometer, shown in Section 1. By the mean normalization ($\mathrm{I_{x\text{-}nom}}$, $\mathrm{I_{y\text{-}nom}}$) for each interferometric signal ($\mathrm{I_x}$, $\mathrm{I_y}$) indicated in Equations (20) and (21), the orthogonal signal with normalization processing can be acquired. In order to illustrate this method, an assumed ellipse is utilized to perform the mean normalization. Its center is in the coordinate (0, 0), the length of the semi-major axis, and the semi-minor axis equal 2 and 1, respectively. The original graph, shown in Figure 6a, can be converted into a circle (Figure 6b) by this normalization. In summary, the reflectance of the coated plane mirror and transmittance of the optical cavity are 0.25 and 0.86.

And the angle of Φ, θ, α_1 and α_2 are π/4, 0, 0, and π/4, respectively. The Lissajous signal of the proposed differential Fabry–Pérot interferometer is demonstrated in Figure 7a,b.

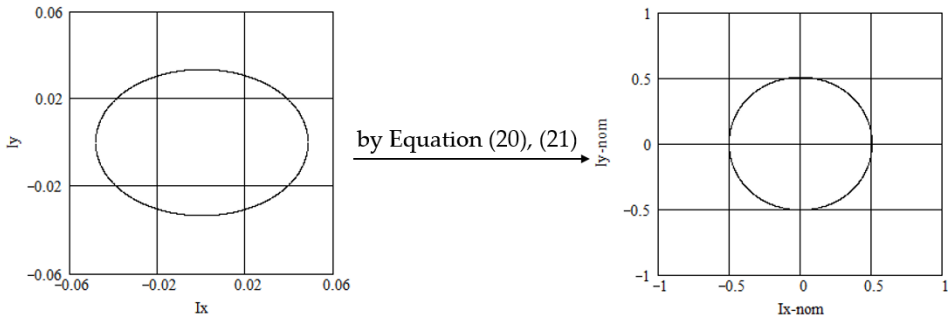
$$I_{x-nom} = \frac{I_x - \mu}{I_{x_max} - I_{x_min}} \tag{20}$$

$$I_{y-nom} = \frac{I_y - \mu}{I_{y_max} - I_{y_min}} \tag{21}$$



(**a**) (**b**)

Figure 6. Assumed ellipse. (**a**) Original graph; (**b**) Graph with mean normalization processing.



(**a**) (**b**)

Figure 7. Orthogonal signal of proposed differential quadrature Fabry–Pérot interferometer. (**a**) Original signal; (**b**) Signal with mean normalization processing.

According to the proposed differential Fabry–Pérot interferometer, the simulated results illustrated in Figure 7 reveal that it is an ellipse orthogonal signal without the DC offset. It means that by subtracting two pairs of the signal with a phase difference of π, the DC offset can be eliminated. Then, the equal AC amplitudes can be realized by the hardware circuit, and that minimized the nonlinearity error. Therefore, by the integration of the differential optical structure, and common path interferometric technique, the DC offset can be eliminated, and the nonlinearity error can also be improved. The analysis of the nonlinearity error is similar to the polarized Fabry–Pérot interferometer. Compared to the polarized structure, the result reveals that the nonlinearity error is significantly reduced to less than one nanometer, which equals to two magnitude orders (Figure 8).

In summary, by the proposed differential measurement structure, the DC offset occurs during the measurement can be eliminated without a complex signal processing module. The nonlinearity error can also be improved significantly to realize the precise industrial and scientific applications.

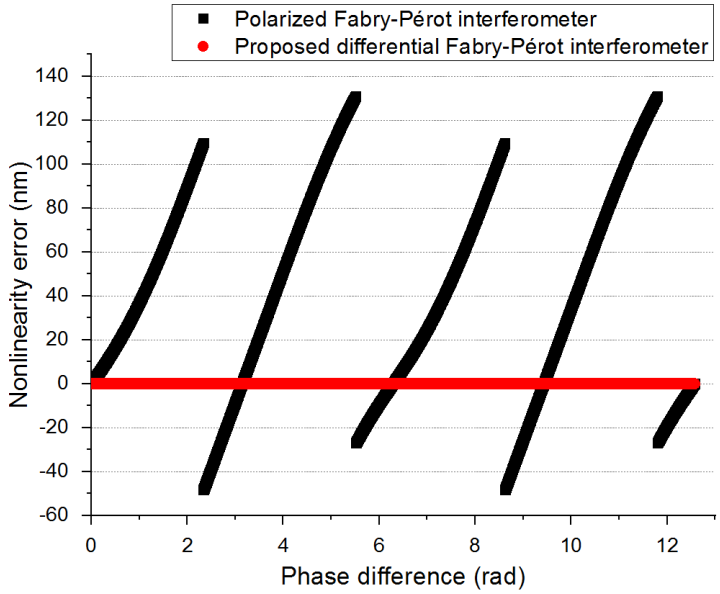


Figure 8. Comparison of nonlinearity error between polarized and proposed differential Fabry–Pérot interferometer.

3. Experimental Results

To verify the measurement performance of the proposed differential quadrature Fabry–Pérot interferometer, a commercial interferometer with the resolution of 1 nm is employed as a reference standard to carry out the comparison experiment simultaneously. After the experiment, the deviation can be obtained by the difference between the measured values of two interferometers. For determining the measurement repeatability, the experimental standard deviation is calculated by 10 deviations (10 repeated cycles) at each position, and then the linearity can be confirmed through dividing three times the maximum standard deviation by the whole measuring range [20]. The experimental arrangement is demonstrated in Figure 9. In this experiment, the measurement structure of PM type in the small measuring range and that of CCR type in the large range have been utilized. Results can be gained in both structures. The Fabry–Pérot interferometer and the commercial interferometer are installed on the left and right sides of the linear stage, and the corresponding measurement mirror is fixed on it to carry out the measurement procedure.

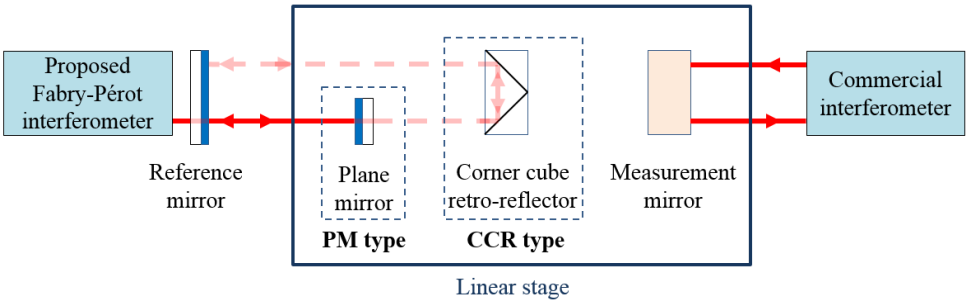


Figure 9. The optical arrangement of the comparison experiment between the commercial and proposed interferometer.

In the comparison experiment between the Fabry–Pérot interferometer of the PM type with the resolution of λ/8 and commercial interferometer, the forward displacement is regulated from 0 mm to 150 mm with a step interval of 15 mm, and each cycle is repeated 10 times. According to the

measurement result (Figure 10), the maximum deviation between the two interferometers is 0.219 μm, the maximum standard deviation is 0.076 μm, and the linearity is 1.52×10^{-6} F.S. in the whole range.

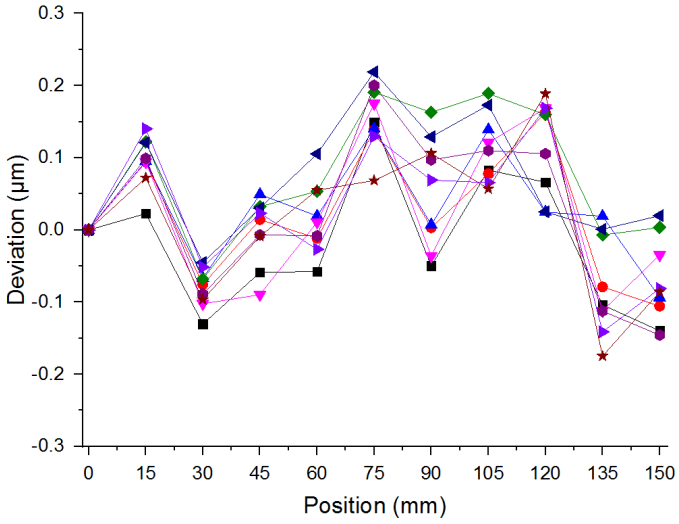


Figure 10. Comparison result between the commercial interferometer and proposed Fabry–Pérot interferometer of PM type.

The comparison experiment between the Fabry–Pérot interferometer of the CCR type with the resolution of λ/16 and commercial interferometer is similar to the above-mentioned procedure. The measuring range is extended to 600 mm, which is conducted with a step interval of 60 mm. The measurement results, shown in Figure 11, demonstrates that the maximum deviation, the maximum standard deviation, and the linearity are 0.427 μm, 0.120 μm, and 6×10^{-7} F.S., respectively. From these comparison results between two measurement types demonstrated in Table 2, the linearity of CCR type is better than the PM type. Because of CCR bearing large tilt angles of the measurement mirror, the linearity of CCR type would be better than that of the PM type within the same measuring range.

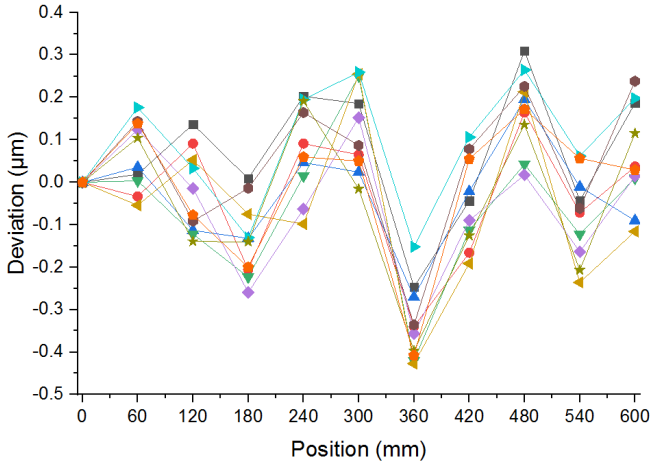


Figure 11. The comparison result between the commercial interferometer and proposed Fabry–Pérot interferometer of CCR type.

In order to evaluate the improvement of the measurement performance in the large measuring range, comparison results between the published polarized Fabry–Pérot interferometer in reference 11 and the proposed differential Fabry–Pérot interferometer of CCR type are illustrated in Table 3. It reveals that the linearity in the published structure within the range of 500 mm is 8.76×10^{-7} F.S.,

and the linearity in the proposed structure within the extended range of 600 mm is 6×10^{-7} F.S. In summary, the maximum deviation and linearity can be improved by 48% and 32%, respectively by the proposed measurement system. This measurement performance can be utilized for the linear displacement measurement to meet the high-precision industrial demand.

Table 2. The comparison result of the proposed measurement structure between the PM type and the CCR type.

Measurement Performance / Type			PM	CCR
Range		mm	150	160
Maximum	standard deviation (σ)	μm	0.076	0.120
	standard deviation (3σ)		0.228	0.360
Linearity ($\frac{3\sigma}{\text{Range}}$)		F.S.	1.52×10^{-6}	6×10^{-7}

Table 3. The comparison result between the published and the proposed measurement structure.

Measurement Performance / Item			Reference 11	Proposed Structure	Improvement (%)
Range		mm	500	600	
Maximum	deviation	μm	0.824	0.427	48
	standard deviation (σ)		0.146	0.120	
	standard deviation (3σ)		0.438	0.360	
Linearity ($\frac{3\sigma}{\text{Range}}$)		F.S.	8.76×10^{-7}	6×10^{-7}	32

4. Conclusions

In this study, the differential quadrature Fabry–Pérot interferometer with variable measurement mirrors for employing in different measuring ranges has been proposed. By the integration of the differential optical structure and common path interferometric technique, the nonlinearity error can be effectively reduced, which equals two magnitude orders, and the DC offset can also be eliminated during the measurement procedure. The measurement performance of the developed Fabry–Pérot interferometer has been verified. From the experimental result, the measurement repeatability is less than 0.120 μm, and the linearity is 6×10^{-7} F.S. within the whole range of 600 mm. By the comparison of the measurement performance between the published polarized Fabry–Pérot interferometer and the proposed differential Fabry–Pérot interferometer, the maximum deviation and linearity can be improved by 48% and 32%, respectively. The capability of the proposed system is conducive to industrial applications to realize the high precision displacement measurement.

Author Contributions: Conceptualization, Y.-C.S., P.-C.T., W.-Y.J., C.-P.C., L.-H.S. and T.-H.H.; Investigation, Y.-C.S., L.-H.S., P.-C.T., W.-Y.J., C.-P.C., T.-H.H.; Writing—original draft, Y.-C.S. and P.-C.T.; Writing—review and editing, P.-C.T., Y.-C.S., W.-Y.J., C.-P.C., L.-H.S. and T.-H.H. All authors have read and agreed to the published version of the manuscript.

Funding: This research was funded by the Ministry of Science and Technology under the Grant number MOST 108-2221-E-224-044, and also by the Ministry of Economic Affairs under the Grant number108-EC-17-A-05-S5-001.

Acknowledgments: For the technical suggestions and the experimental analyses, authors would like to be grateful to Prof. Yung-Cheng Wang and Mr. Teng-Chi Wu in National Yunlin University of Science and Technology. We acknowledge the financial support by the Ministry of Science and Technology under the Grant number MOST 108-2221-E-224-044, and also by the Ministry of Economic Affairs under the Grant number108-EC-17-A-05-S5-001.

Conflicts of Interest: The authors declare no conflict of interest.

References

1. John, L.; Ernest, K. Michelson interferometry with 10 pm accuracy. *Rev. Sci. Instrum.* **2000**, *71*, 2669.

2. Gerd, J. Three-Dimensional Nanopositioning, Nanomeasuring Machine with a Resolution of 0.1 nm. *Optoelectron. Instrum. Data Proc.* **2010**, *46*, 318–323.
3. Walter, D.P. Inference of cosmological parameters from gravitational waves: Applications to second generation interferometers. *Phys. Rev. D* **2011**, *86*, 3011.
4. Gargi, R. Atomic Force Microscopy as a Nanometrology Tool: Some Issues and Future Targets. *Mapan* **2013**, *28*, 311–319.
5. Pietraszewski, K.A.R.B. Recent Developments in Fabry-Pérot Interferometer. *ASP Conf. Ser.* **2000**, *195*, 591–596.
6. John, R.L. Fabry-Pérot metrology for displacements up to 50 mm. *J. Opt. Soc. Am. A Opt. Image. Sci. Vis.* **2005**, *22*, 2786–2798.
7. Wang, Y.C.; Shyu, L.H.; Chang, C.P. The Comparison of Environmental Effects on Michelson and Fabry-Perot Interferometers Utilized for the Displacement Measurement. *Sensors* **2010**, *10*, 2577–2586. [CrossRef] [PubMed]
8. Vaughan, J.M. *Fabry–Perot Interferometer History Theory Practice and Applications*; Adam Hilger: Bristol, UK; Boca Raton, FL, USA, 1989; pp. 1–43.
9. Murphy, K.A.; Gunther, M.F.; Vengsarkar, A.M.; Claus, R.O. Quadrature phase-shifted, extrinsic Fabry–Perot optical fiber sensors. *Opt. Lett.* **1991**, *16*, 273–275. [CrossRef] [PubMed]
10. Chang, C.P.; Tung, P.C.; Shyu, L.H.; Wang, Y.C.; Manske, E. Fabry–Perot displacement interferometer for the measuring range up to 100 mm. *Measurements* **2013**, *46*, 4094–4099. [CrossRef]
11. Chang, C.P.; Tung, P.C.; Shyu, L.H.; Wang, Y.C.; Manske, E. Modified Fabry-Perot interferometer for displacement measurement in ultra large measuring range. *Rev. Sci. Instr.* **2013**, *84*, 053105. [CrossRef] [PubMed]
12. Shyu, L.H.; Chang, C.P.; Wang, Y.C. Influence of intensity loss in the cavity of a folded Fabry-Perot interferometer on interferometric signals. *Rev. Sci. Instr.* **2011**, *82*, 063103. [CrossRef] [PubMed]
13. Cui, J.; He, Z.; Jiu, Y.; Tan, J.; Sun, T. Homodyne laser interferometer involving minimal quadrature phase error to obtain subnanometer nonlinearity. *Appl. Opt.* **2016**, *55*, 55. [CrossRef] [PubMed]
14. Fu, H.; Ji, R.; Hu, P.; Wang, Y.; Wu, G.; Tan, J. Measurement Method for Nonlinearity in Heterodyne Laser Interferometers Based on Double-Channel Quadrature Demodulation. *Sensors* **2018**, *18*, 2768. [CrossRef] [PubMed]
15. Hu, P.; Zhu, J.; Zhai, X.; Tan, J. DC-offset-free homodyne interferometer and its nonlinearity compensation. *Opt. Express* **2015**, *23*, 8399–8408. [CrossRef] [PubMed]
16. Heydemann, P.L.M. Determination and correction of quadrature fringe measurement errors in interferometers. *Appl. Opt.* **1981**, *20*, 3382–3384. [CrossRef] [PubMed]
17. Eom, T.; Kim, J.; Jeong, K. The dynamic compensation of nonlinearity in a homodyne laser interferometer. *Meas. Sci. Technol.* **2001**, *12*, 1734–1738. [CrossRef]
18. Shyu, L.H.; Wang, Y.C.; Chang, C.P.; Shih, Y.C.; Manske, E. A signal interpolation method for Fabry–Perot interferometer utilized in mechanical vibration measurement. *Measurements* **2016**, *92*, 83–88. [CrossRef]
19. Rabinowitz, P.; Jacobs, S.F.; Shultz, T.; Gould, G. Cube-Corner Fabry-Perot Interferometer. *J. Opt. Soc. Am.* **1962**, *52*, 452. [CrossRef]
20. Enderton, H.B. Vladimir A. Uspensky. Godel's incompleteness theorem. A reprint of LV 889 with minor corrections. Theoretical computer science, vol. 130 (1994), pp. 239–319. *J. Symb. Log.* **1995**, *60*, 1320. [CrossRef]



© 2020 by the authors. Licensee MDPI, Basel, Switzerland. This article is an open access article distributed under the terms and conditions of the Creative Commons Attribution (CC BY) license (http://creativecommons.org/licenses/by/4.0/).